arXiv:1506.00324v1 [hep-ph] 1 Jun 2015

Localized direct CP violation in $B^{\pm} \to \rho^0(\omega)\pi^{\pm} \to \pi^+\pi^-\pi^{\pm}$

Chao Wang,[1,*] Zhen-Hua Zhang,[2,†] Zhen-Yang Wang,[1,‡] and Xin-Heng Guo[1,§]

[1] *College of Nuclear Science and Technology, Beijing Normal University, Beijing 100875, China*

[2] *School of Nuclear Science and Technology, University of South China, Hengyang HUNAN 421001, China*

Abstract

We study the localized direct CP violation in the hadronic decays $B^{\pm} \to \rho^0(\omega)\pi^{\pm} \to \pi^+\pi^-\pi^{\pm}$, including the effect caused by an interesting mechanism involving the charge symmetry violating mixing between ρ^0 and ω. We calculate the localized integrated direct CP violation when the low invariant mass of $\pi^+\pi^-$ $[m(\pi^+\pi^-)_{low}]$ is near $\rho^0(770)$. For five models of form factors investigated, we find that the localized integrated direct CP violation varies from -0.0170 to -0.0860 in the ranges of parameters in our model when $0.750 < m(\pi^+\pi^-)_{low} < 0.800\,\text{GeV}$. This result, especially the sign, agrees with the experimental data and is independent of form factor models. The new experimental data shows that the signs of the localized integrated CP asymmetries in the regions $0.470 < m(\pi^+\pi^-)_{low} < 0.770\,\text{GeV}$ and $0.770 < m(\pi^+\pi^-)_{low} < 0.920\,\text{GeV}$ are positive and negative, respectively. We find that ρ-ω mixing makes the localized integrated CP asymmetry move towards the negative direction, and therefore contributes to the sign change in those two regions. This behavior is also model independent. We also calculate the localized integrated direct CP violating asymmetries in the regions $0.470 < m(\pi^+\pi^-)_{low} < 0.770\,\text{GeV}$ and $0.770 < m(\pi^+\pi^-)_{low} < 0.920\,\text{GeV}$ and find that they agree with the experimental data in some models of form factors.

PACS numbers: 11.30.Er, 12.39.-x, 13.25.Hw

* Email:chaowang11@mail.bnu.edu.cn

† Email:zhangzh@usc.edu.cn

‡ Email:rongtian@mail.bnu.edu.cn

§ Corresponding author, Email:xhguo@bnu.edu.cn

I. INTRODUCTION

CP violation is one of the most fundamental and important properties of weak interactions. Even though it has been known since 1964 [1], we still do not know the source of CP violation completely. In the Standard Model, CP violation is originated from the weak phase in the Cabibbo-Kobayashi-Maskawa (CKM) matrix [2, 3]. Besides the weak phase, a large strong phase is also needed for direct CP violation to occur in decay processes. Usually, this large phase is provided by QCD loop corrections and some phenomenological mechanisms. In the past few years, numerous theoretical studies have been conducted on CP violation. However, we need a lot of data to test these approaches because there are many theoretical uncertainties such as CKM matrix elements, hadronic matrix elements and nonfactorizable effects. These uncertainties would be reduced by the increase of experimental data in the future.

Recently, LHCb Collaboration focused on three-body final states in the decays of B and D mesons and a novel strategy to probe CP asymmetry in their Dalitz plots [4–6]. The local asymmetries in specific regions of the phase space of charmless three-body decays of bottom mesons, such as $B^\pm \to \pi^\pm\pi^+\pi^-$ and $B^\pm \to K^\pm\pi^+\pi^-$, were measured. It was shown that the local asymmetry distributions in the Dalitz plots reveal rich structures and are not uniform [4–6]. These intriguing discoveries offer opportunities to search for different sources of CP violation, through the study of the signatures of these sources in certain phase spaces of the Dalitz plots. In fact, several theoretical studies have been made to explain these distributions, such as the interference between intermediate states [7, 8] and final-state rescatterings [6, 9, 10]. One can confirm that these complex structures originate from more than one source [6].

In previous works, an interesting phenomenological mechanism involving the charge symmetry violating mixing between ρ^0 and ω (ρ-ω mixing) was considered to obtain a large strong phase in B decays [11–13] and it was found that such a mixing can lead to a peak of CP violation when the invariant mass of $\pi^+\pi^-$ is near ω. The differential CP asymmetry was studied in the decays $B^\pm \to \rho^0(\omega)\pi^\pm \to \pi^+\pi^-\pi^\pm$ before [14]. ρ-ω mixing provides additional complex terms to the amplitudes [15] and the strong phase passes through 90° at the ω resonance. In our previous work, we found that it is more useful to investigate the localized integrated CP asymmetry and studied the localized integrated CP asymme-

try in hadronic τ decays with this mechanism [15]. The newest LHCb experiments showed that the resonances are $\rho^0(770)$ when $m^2(\pi^+\pi^-)_{low} < 1\mathrm{GeV}^2/\mathrm{c}^4$ for $B^\pm \to \pi^+\pi^-\pi^\pm$ decays [$m(\pi^+\pi^-)_{low}$ is the low invariance mass of $\pi^+\pi^-$] [6]. It was claimed that the CP asymmetry in these decays changes sign around the $\rho^0(770)$ peak of $m^2(\pi^+\pi^-)_{low}$ [6], which contains the significant region of ρ-ω mixing. In the present paper, we aim at studying the localized integrated CP asymmetry in $B^\pm \to \pi^+\pi^-\pi^\pm$ decays involving ρ-ω mixing and comparing it with the results obtained from LHCb Collaboration.

In this paper, we will investigate the localized integrated CP violation with five phenomenological models of weak form factors for $B^\pm \to \rho^0(\omega)\pi^\pm \to \pi^-\pi^+\pi^\pm$ with and without ρ-ω mixing. We will determine the allowed range of N_c which is the effective color number describing nonfactorizable contributions. The model dependence of our results will be discussed in detail. We will see that for five models of form factors, our result for the localized integrated CP asymmetry varies from -0.0295 (-0.0170) to -0.0860 (-0.0585) in the ranges of N_c, $2.78(2.85) < N_c < 9.68(9.02)$ corresponding to $q^2/m_b^2 = 0.3(0.5)$ (q is the typical momentum transfer of the gluon or photon in the penguin diagrams) when $0.750 < m(\pi^+\pi^-)_{low} < 0.800\,\mathrm{GeV}$. Form Fig. 4 of Ref. [6], we can see the localized integrated CP asymmetries have different signs in $\cos\theta > 0$ and $\cos\theta < 0$ regions when $0.750 < m(\pi^+\pi^-)_{low} < 0.800\,\mathrm{GeV}$ (θ is the angle between the momenta of the unpaired $\pi^{+(-)}$ and the ρ^0 decay product with the same-sign charge). If one adds the events in these two experimental regions together, the total localized integrated CP asymmetry will be -0.0294 ± 0.0285. Our results agree with this experimental data. The experimental values of the localized integrated CP asymmetries in the regions $0.470 < m(\pi^+\pi^-)_{low} < 0.770\,\mathrm{GeV}$ and $0.770 < m(\pi^+\pi^-)_{low} < 0.920\,\mathrm{GeV}$ are 0.0508 ± 0.0171 and -0.0256 ± 0.0202, respectively, with opposite signs [6]. We will find that ρ-ω mixing can make the localized integrated CP asymmetry move towards the negative direction, and therefore will contribute to the sign change from the region $0.470 < m(\pi^+\pi^-)_{low} < 0.770\,\mathrm{GeV}$ to $0.770 < m(\pi^+\pi^-)_{low} < 0.920\,\mathrm{GeV}$. This behavior is model independent. Furthermore, we will find that our results in these two regions are consistent with the experimental data for serval models of form factors.

The remainder of this paper is organized as follows. In Sec. II, we present the form of the effective Hamiltonian and the values of Wilson coefficients and give the formalism for the CP violating asymmetry in $B^\pm \to \rho^0(\omega)\pi^\pm \to \pi^+\pi^-\pi^\pm$. Then we show numerical results

with several models of form factors in this section. In Sec. III, we calculate branching ratios for $B^+ \to \rho^0\pi^+$ and $B^0 \to \rho^+\pi^-$ and present numerical results for the range of N_c allowed by the experimental data. In the last section, we give some discussions and summarize our results.

II. CP VIOLATION IN $B^\pm \to \rho^0(\omega)\pi^\pm \to \pi^+\pi^-\pi^\pm$

The amplitude of a decay process described by some amplitudes may have CP-even and -odd relative phases. Within the Stand Model, the CP-odd relative phase is always a weak phase difference which is directly determined by the CKM matrix. On the other hand, CP-even phases, which are called strong phases, are usually originated from non-perturbative effects of strong interactions and are hard to handle. We consider a B meson weak decay process, $B \to M_1M_2M_3$, where $M_i(i = 1, 2, 3)$ is a light pseudoscalar meson. For a weak decay process of a heavy meson, a typical form of the decay amplitude A and its CP conjugate one $\bar{A}$ are

$$A = g_1 r_1 \mathrm{e}^{\mathrm{i}\phi_1} + g_2 r_2 \mathrm{e}^{\mathrm{i}\phi_2}, \tag{1}$$

$$\bar{A} = g_1^* r_1 \mathrm{e}^{\mathrm{i}\phi_1} + g_2^* r_2 \mathrm{e}^{\mathrm{i}\phi_2}, \tag{2}$$

where g_1 and g_2 represent CP-odd complex terms which involve CKM matrix elements, $r_1 e^{\mathrm{i}\phi_1}$ and $r_2 e^{\mathrm{i}\phi_2}$ terms are even under the CP transformation. Then, one has

$$\begin{aligned} |A|^2 - |\bar{A}|^2 &= 4 r_1 r_2\, \mathfrak{Im}(g_1^* g_2)\, \sin(\phi_1 - \phi_2) \\ &= 4 r_1 r_2 |g_1||g_2|\, \sin[\,\mathrm{Arg}(g_2/g_1)]\, \sin(\phi_1 - \phi_2), \end{aligned} \tag{3}$$

from which, we can see explicitly that both the CP-odd phase difference $\mathrm{Arg}(g_2/g_1)$ and the CP-even phase difference $\phi_1 - \phi_2$ are needed to produce CP violation.

A. The effective Hamiltonian

In order to calculate the direct CP violating asymmetry in hadronic decays, one can use the following effective weak Hamiltonian based on the Operator Product Expansion [16]:

$$\mathcal{H} = \frac{G_F}{\sqrt{2}} \big[V_{ub} V_{ud}^* (c_1 O_1^u + c_2 O_2^u) - V_{tb} V_{td}^* \sum_{i=3}^{10} c_i O_i \big] + H.c., \tag{4}$$

where V_{ub}, V_{ud}, V_{tb} and V_{td} are CKM matrix elements, and $c_i (i = 1, ..., 10)$ are the Wilson coefficients, which are calculable in the renormalization group improved perturbation theory and are scale dependent. In the present case, we work with the renormalization scheme independent Wilson coefficients and use the values of the Wilson coefficients at the renormalization scale $\mu \approx m_b$. The operators O_i have the following forms:

$$
\begin{aligned}
O_1^u &= \overline{d}_\alpha \gamma_\mu (1-\gamma_5) u_\beta \overline{u}_\beta \gamma^\mu (1-\gamma_5) b_\alpha, \\
O_2^u &= \overline{d} \gamma_\mu (1-\gamma_5) u \overline{u} \gamma^\mu (1-\gamma_5) b, \\
O_3 &= \overline{d} \gamma_\mu (1-\gamma_5) b \sum_{q'} \overline{q'} \gamma^\mu (1-\gamma_5) q', \\
O_4 &= \overline{d}_\alpha \gamma_\mu (1-\gamma_5) b_\beta \sum_{q'} \overline{q'}_\beta \gamma^\mu (1-\gamma_5) q'_\alpha, \\
O_5 &= \overline{d} \gamma_\mu (1-\gamma_5) b \sum_{q'} \overline{q'} \gamma^\mu (1+\gamma_5) q', \\
O_6 &= \overline{d}_\alpha \gamma_\mu (1-\gamma_5) b_\beta \sum_{q'} \overline{q'}_\beta \gamma^\mu (1+\gamma_5) q'_\alpha, \\
O_7 &= \frac{3}{2} \overline{d} \gamma_\mu (1-\gamma_5) b \sum_{q'} e_{q'} \overline{q'} \gamma^\mu (1+\gamma_5) q', \\
O_8 &= \frac{3}{2} \overline{d}_\alpha \gamma_\mu (1-\gamma_5) b_\beta \sum_{q'} e_{q'} \overline{q'}_\beta \gamma^\mu (1+\gamma_5) q'_\alpha, \\
O_9 &= \frac{3}{2} \overline{d} \gamma_\mu (1-\gamma_5) b \sum_{q'} e_{q'} \overline{q'} \gamma^\mu (1-\gamma_5) q', \\
O_{10} &= \frac{3}{2} \overline{d}_\alpha \gamma_\mu (1-\gamma_5) b_\beta \sum_{q'} e_{q'} \overline{q'}_\beta \gamma^\mu (1-\gamma_5) q'_\alpha,
\end{aligned}
\tag{5}
$$

where α and β are color indices, and $q' = u, d$ or s quarks. In Eq. (5), O_1^u and O_2^u are the tree level operators, $O_3 - O_6$ are QCD penguin operators, and $O_7 - O_{10}$ arise from electroweak penguin diagrams.

The Wilson coefficients, c_i, which are known to the next-to-leading logarithmic order, take the following values [17, 18]:

$$
\begin{aligned}
&c_1 = -0.3125, \qquad c_2 = 1.1502, \\
&c_3 = 0.0174, \qquad c_4 = -0.0373, \\
&c_5 = 0.0104, \qquad c_6 = -0.0459, \\
&c_7 = -1.050 \times 10^{-5}, \qquad c_8 = 3.839 \times 10^{-4}, \\
&c_9 = -0.0101, \qquad c_{10} = 1.959 \times 10^{-3},
\end{aligned} \tag{6}
$$

at the scale $\mu = m_b = 5\,\mathrm{GeV}$.

To be consistent, the matrix elements of the operators O_i should also be renormalized to the one-loop order. This results in the effective Wilson coefficients, c_i', which satisfy the constraint

$$
c_i(m_b)\langle O_i(m_b)\rangle = c_i'\langle O_i\rangle^{tree}, \tag{7}
$$

where $\langle O_i\rangle^{tree}$ is the matrix element at the tree level, which will be evaluated in the factorization approach. From Eq. (7), the relations between c_i' and c_i are [17, 18]

$$
\begin{aligned}
&c_1' = c_1, \qquad c_2' = c_2, \\
&c_3' = c_3 - P_s/3, \qquad c_4' = c_4 + P_s, \\
&c_5' = c_5 - P_s/3, \qquad c_6' = c_6 + P_s, \\
&c_7' = c_7 + P_e, \qquad c_8' = c_8, \\
&c_9' = c_9 + P_e, \qquad c_{10}' = c_{10},
\end{aligned} \tag{8}
$$

where

$$
\begin{aligned}
P_s &= (\alpha_s/8\pi)c_2[10/9 + G(m_c, \mu, q^2)], \\
P_e &= (\alpha_{em}/9\pi)(3c_1 + c_2)[10/9 + G(m_c, \mu, q^2)],
\end{aligned}
$$

with

$$
G(m_c, \mu, q^2) = 4\int_0^1 \mathrm{d}x x(x-1)\ln\frac{m_c^2 - x(1-x)q^2}{\mu^2}.
$$

$G(m_c, \mu, q^2)$ has the following explicit expression [29]:

$$\mathfrak{Re}G = \frac{2}{3}\left[\ln\frac{m_c^2}{\mu^2} - \frac{5}{3} - 4\frac{m_c^2}{q^2} + \left(1 + 2\frac{m_c^2}{q^2}\right) \times \sqrt{1 - 4\frac{m_c^2}{q^2}} \ln\frac{1 + \sqrt{1 - 4\frac{m_c^2}{q^2}}}{1 - \sqrt{1 - 4\frac{m_c^2}{q^2}}}\right],$$

$$\mathfrak{Im}G = -\frac{2}{3}\left(1 + 2\frac{m_c^2}{q^2}\right)\sqrt{1 - 4\frac{m_c^2}{q^2}}. \tag{9}$$

Based on simple arguments at the quark level, the value of q^2 is chosen to be in the range $0.3 < q^2/m_b^2 < 0.5$ [11]. From Eqs. (8) and (9) we can obtain numerical values for c_i'.

When $q^2/m_b^2 = 0.3$,

$$\begin{aligned}
c_1' &= -0.3125, \qquad c_2' = 1.1502, \\
c_3' &= 2.433 \times 10^{-2} + 1.543 \times 10^{-3}\mathrm{i}, \\
c_4' &= -5.808 \times 10^{-2} - 4.628 \times 10^{-3}\mathrm{i}, \\
c_5' &= 1.733 \times 10^{-2} + 1.543 \times^{-3} \mathrm{i}, \\
c_6' &= -6.668 \times 10^{-2} - 4.628 \times^{-3} \mathrm{i}, \\
c_7' &= -1.435 \times 10^{-4} - 2.963 \times^{-5} \mathrm{i}, \\
c_8' &= 3.839 \times 10^{-4}, \\
c_9' &= -1.023 \times 10^{-2} - 2.963 \times^{-5} \mathrm{i}, \\
c_{10}' &= 1.959 \times 10^{-3},
\end{aligned} \tag{10}$$

and when $q^2/m_b^2 = 0.5$, one has

$$\begin{aligned}
c_1' &= -0.3125, \qquad c_2' = 1.1502, \\
c_3' &= 2.120 \times 10^{-2} + 2.174 \times 10^{-3}\mathrm{i}, \\
c_4' &= -4.869 \times 10^{-2} - 1.552 \times 10^{-3}\mathrm{i}, \\
c_5' &= 1.420 \times 10^{-2} + 5.174 \times^{-3} \mathrm{i}, \\
c_6' &= -5.729 \times 10^{-2} - 1.552 \times^{-2} \mathrm{i}, \\
c_7' &= -8.340 \times 10^{-5} - 9.938 \times^{-5} \mathrm{i}, \\
c_8' &= 3.839 \times 10^{-4}, \\
c_9' &= -1.017 \times 10^{-2} - 9.938 \times^{-5} \mathrm{i}, \\
c_{10}' &= 1.959 \times 10^{-3},
\end{aligned} \tag{11}$$

where we have taken $\alpha_s(m_Z) = 0.112$, $\alpha_{em}(m_b) = 1/132.2$, $m_b = 5\,\mathrm{GeV}$, and $m_c = 1.35\,\mathrm{GeV}$.

B. Formalism

The amplitude for the decay $B^- \to \pi^+\pi^-\pi^-$ through the vector resonance (ρ^0 and ω) can be expressed as [14, 19]:

$$A = (\Sigma - s')\mathcal{M} = \langle\pi^+\pi^-\pi^-|H^T|B^-\rangle + \langle\pi^+\pi^-\pi^-|H^P|B^-\rangle, \tag{12}$$

where H^T and H^P are the Hamiltonians for the tree and penguin operators, respectively, $\Sigma - s'$ is a term which accounts for angular momentum conservation when the spin of the resonance is 1, $\sqrt{s'}$ is the high invariance mass of the $\pi^+\pi^-$ pair, $\Sigma = \frac{1}{2}(s'_{max} + s'_{min})$ with s'_{max} and s'_{min} being the maximum and minimum values of s' for a fixed s, respectively, and $\sqrt{s}$ is the low invariant mass of the $\pi^+\pi^-$ pair $[m(\pi^+\pi^-)_{low}]$. In order to obtain a large signal for direct CP violation, we need to appeal to some phenomenological mechanisms. ρ-ω mixing has the dual advantages that the strong phase difference is large (passes through 90° at the ω resonance) and well known [12, 13]. With this mechanism, to the first order in isospin violation, the amplitude for $B^- \to \rho^0(\omega)\pi^- \to \pi^+\pi^-\pi^-$ takes the following form at a value of $\sqrt{s}$ close to the ω resonance mass [14]:

$$\langle\pi^+\pi^-\pi^-|H^T|B^-\rangle = (\Sigma - s')\left(\frac{g_\rho}{s_\rho s_\omega}\tilde{\Pi}_{\rho\omega}t_\omega + \frac{g_\rho}{s_\rho}t_\rho\right), \tag{13}$$

$$\langle\pi^+\pi^-\pi^-|H^P|B^-\rangle = (\Sigma - s')\left(\frac{g_\rho}{s_\rho s_\omega}\tilde{\Pi}_{\rho\omega}p_\omega + \frac{g_\rho}{s_\rho}p_\rho\right), \tag{14}$$

where t_V ($V = \rho^0$ or ω) is the tree amplitude and p_V is the penguin amplitude for producing an intermediate vector meson V, g_ρ is the coupling for $\rho^0 \to \pi^+\pi^-$, $\tilde{\Pi}_{\rho\omega}$ is the effective ρ-ω mixing amplitude, and s_V is from the inverse propagator of the vector meson V,

$$s_V = s - m_V^2 + \mathrm{i}m_V\Gamma_V. \tag{15}$$

From Eqs. (13) and (14), we note that ρ-ω mixing provides an additional complex term for the tree and penguin amplitudes (the first term in each equation), respectively. These complex terms will enlarge the CP-even phase, and lead to a peak of CP asymmetry as mentioned before. We will show the difference between the CP asymmetries with and without ρ-ω mixing later. Here, we assume that the $B^\pm \to \pi^+\pi^-\pi^\pm$ process is dominated by the resonance ρ^0 in certain region of its Dalitz plot.

We stress that the direct coupling $\omega \to \pi^+\pi^-$ is effectively absorbed into $\tilde{\Pi}_{\rho\omega}$ [20], leading to the explicit s dependence of $\tilde{\Pi}_{\rho\omega}$. Making the expansion $\tilde{\Pi}_{\rho\omega}(s) = \tilde{\Pi}_{\rho\omega}(m_\omega) +$

$(s-m_\omega)\tilde{\Pi}'_{\rho\omega}(m_\omega)$, the ρ-ω mixing parameters were determined in the fit of Gardner and O'Connell [21]:

$$\begin{aligned}\mathfrak{Re}\tilde{\Pi}_{\rho\omega}(m_\omega^2) &= -3500\pm 300\ \mathrm{MeV}^2,\\ \mathfrak{Im}\tilde{\Pi}_{\rho\omega}(m_\omega^2) &= -300\pm 300\ \mathrm{MeV}^2,\\ \tilde{\Pi}'_{\rho\omega}(m_\omega^2) &= 0.03\pm\ 0.04.\end{aligned} \tag{16}$$

In practice, the effect of the derivative term is negligible.

In this work, we only consider ρ^0 and ω resonances. Then, for a fixed s, the differential CP asymmetry parameter can be defined as

$$A_{CP}=\frac{|\mathcal{M}|^2-|\bar{\mathcal{M}}|^2}{|\mathcal{M}|^2+|\bar{\mathcal{M}}|^2}. \tag{17}$$

By integrating the denominator and numerator of A_{CP}, respectively, in the region Ω ($s_1<s<s_2$, $s'_1<s'<s'_2$), we obtain the localized integrated CP asymmetry, which can be measured by experiments and takes the following form:

$$A_{CP}^{\Omega}=\frac{\int_{s_1}^{s_2}\mathrm{d}s\int_{s'_1}^{s'_2}\mathrm{d}s'(\Sigma-s')^2(|\mathcal{M}|^2-|\bar{\mathcal{M}}|^2)}{\int_{s_1}^{s_2}\mathrm{d}s\int_{s'_1}^{s'_2}\mathrm{d}s'(\Sigma-s')^2(|\mathcal{M}|^2+|\bar{\mathcal{M}}|^2)}. \tag{18}$$

According to kinematics of the three body decay, $\Sigma[=\frac{1}{2}(s'_{max}+s'_{min})]$ is related to s. In our calculations, s varies in a small region, and therefore Σ can be treated as a constant approximately [6]. Then, the terms $\int_{s'_1}^{s'_2}\mathrm{d}s'(\Sigma-s')^2$ are cancelled, and A_{CP}^{Ω} becomes independent of the high invariance mass of $\pi^+\pi^-$. In practice, to be more precise, we take into account the s-dependence of s'_{max} and s'_{min} in our calculations. We choose $s'_{min}<s'<s'_{max}$ as the integration interval of the high invariance mass of $\pi^+\pi^-$ and regard $\int_{s'_{min}}^{s'_{max}}\mathrm{d}s'(\Sigma-s')^2$ as a factor which is dependent on s.

C. Calculational details

With the Hamiltonian given in Eq. (4), we are ready to evaluate the matrix elements for $B^-\to\rho^0(\omega)\pi^-$. In the factorization approximation, either $\rho^0(\omega)$ or π^- is generated by one current which has appropriate quantum numbers in the Hamiltonian. For this decay process, two kinds of matrix element products are involved after factorization: $\langle\rho^0(\omega)|J^\mu|0\rangle\langle\pi^-|J_\mu|B^-\rangle$ and $\langle\pi^-|J^\mu|0\rangle\langle\rho^0(\omega)|J_\mu|B^-\rangle$. We will calculate them in some phenomenological quark models.

The matrix elements for $B \to P$ and $B \to V$ (where P and V denote pseudoscalar and vector mesons, respectively) can be decomposed as [22]

$$\langle P|J_\mu|B\rangle = \Big(p_B + p_P - \frac{m_B^2 - m_P^2}{k^2}\Big)_\mu F_1^{BP}(k^2) + \frac{m_B^2 - m_P^2}{k^2} k_\mu F_0^{BP}(k^2), \tag{19}$$

$$\begin{aligned}\langle V|J_\mu|B\rangle = &\frac{2}{m_B + m_V}\varepsilon_{\mu\nu\rho\sigma}\epsilon^{*\nu} p_B^\rho p_V^\sigma V^{BV}(k^2) + \mathrm{i}\Big\{\epsilon_\mu^*(m_B + m_V)A_1^{BV}(k^2) \\ &-\frac{\epsilon^* \cdot k}{m_B + m_V}(p_B + p_V)_\mu A_2^{BV}(k^2) - \frac{\epsilon^* \cdot k}{k^2} 2m_V \cdot k_\mu A_3^{BV}(k^2)\Big\} \\ &+\mathrm{i}\frac{\epsilon^* \cdot k}{k^2} 2m_V \cdot k_\mu A_0^{BV}(k^2),\end{aligned} \tag{20}$$

where J_μ is the weak current $[J_\mu = \bar{u}\gamma_\mu(1-\gamma_5)b$ or $\bar{d}\gamma_\mu(1-\gamma_5)b]$, $k = p_B - p_{P(V)}$, and ϵ_μ is the polarization vector of V. The form factors included in our calculations satisfy $F_1^{BP}(0) = F_0^{BP}(0)$, $A_3^{BV}(0) = A_0^{BV}(0)$, and $A_3^{BV}(k^2) = [(m_B + m_V)/2m_V]A_1^{BV}(k^2) - [(m_B - m_V)/2m_V]A_2^{BV}(k^2)$. We define the notation X for matrix elements. For example, $X^{(B^-\rho^0,\pi^-)}$ is defined as $\langle\pi^-|\bar{d}\gamma^\mu(1-\gamma_5)u|0\rangle\langle\rho^0|\bar{u}\gamma_\mu(1-\gamma_5)b|B^-\rangle$. These matrix elements can be parameterized as the products of decay constants and form factors. Therefore, the factorized terms $X^{(BM_1,M_2)}$ have the following expressions [23]:

$$\begin{aligned}X^{(BP,V)} &= \langle V|\bar{q}_2\gamma^\mu(1-\gamma_5)q_3|0\rangle\langle P|\bar{q}_1\gamma_\mu(1-\gamma_5)b|B\rangle \\ &= 2f_V m_V F_1^{BP}(m_V^2)(\epsilon^* \cdot p_B),\end{aligned} \tag{21}$$

$$\begin{aligned}X^{(BV,P)} &= \langle P|\bar{q}_2\gamma^\mu(1-\gamma_5)q_3|0\rangle\langle V|\bar{q}_1\gamma_\mu(1-\gamma_5)b|B\rangle \\ &= 2f_P m_V A_0^{BV}(m_P^2)(\epsilon^* \cdot p_B),\end{aligned} \tag{22}$$

where f_V and f_P are the decay constants of vector and pseudoscalar mesons, respectively. Using the decomposition in Eqs. (19)-(22), one has

$$t_\rho = V_{ub}V_{ud}^*\left(a_1\frac{X^{(B^-\rho^0,\pi^-)}}{\epsilon^* \cdot p_B} + a_2\frac{X^{(B^-\pi^-,\rho^0)}}{\epsilon^* \cdot p_B}\right), \tag{23}$$

$$t_\omega = V_{ub}V_{ud}^*\left(a_1\frac{X^{(B^-\omega,\pi^-)}}{\epsilon^* \cdot p_B} + a_2\frac{X^{(B^-\pi^-,\omega)}}{\epsilon^* \cdot p_B}\right), \tag{24}$$

where all the a_i's are built up from the effective Wilson coefficients c_i''s, and take the form $a_i = c_i' + c_{i+1}'/N_c$ for odd i and $a_i = c_i' + c_{i-1}'/N_c$ for even i. It is noted that in the factorization approach, N_c includes nonfactorizable contributions effectively, and the value of N_c should be determined by experiments since we can not evaluate nonfactorizable contributions. In

the same way, we obtain the penguin operator contributions:

$$p_\rho = -V_{tb}V_{td}^*\Bigg\{\Big[-a_4+\frac{3}{2}a_7+\frac{3}{2}a_9+\frac{1}{2}a_{10}\Big]\frac{X^{(B^-\pi^-,\rho^0)}}{\epsilon^*\cdot p_B}$$
$$+\Big[a_4+a_{10}-2(a_6+a_8)\frac{m_\pi^2}{(m_d+m_u)(m_b+m_u)}\Big]\frac{X^{(B^-\rho^0,\pi^-)}}{\epsilon^*\cdot p_B}\Bigg\}, \tag{25}$$

$$p_\omega = -V_{tb}V_{td}^*\Bigg\{\Big[2a_3+a_4+2a_5+\frac{1}{2}(a_7+a_9-a_{10})\Big]\frac{X^{(B^-\pi^-,\omega)}}{\epsilon^*\cdot p_B}$$
$$+\Big[a_4+a_{10}-2(a_6+a_8)\frac{m_\pi^2}{(m_d+m_u)(m_b+m_u)}\Big]\frac{X^{(B^-\omega,\pi^-)}}{\epsilon^*\cdot p_B}\Bigg\}. \tag{26}$$

We adapt the same decay constants and form factors for the matrix elements producing ρ^0 and ω mesons. Then, we have $X^{(B^-\rho^0,\pi^-)} = X^{(B^-\omega,\pi^-)} = 2f_\pi m_\rho A_0(m_\pi^2)(\epsilon^*\cdot p_B)$ and $X^{(B^-\pi^-,\rho^0)} = X^{(B^-\pi^-,\omega)} = \sqrt{2}f_\rho m_\rho F_1(m_\rho^2)(\epsilon^*\cdot p_B)$, where $\langle\rho^0(\omega)|J^\mu|0\rangle = 1/\sqrt{2}f_\rho m_\rho\epsilon^{*\mu}$ and $\langle\pi^-|J_\mu|0\rangle = \mathrm{i}f_\pi p_\mu$.

D. Numerical results

In our numerical calculations we have several parameters: q^2, N_c, and the CKM matrix elements in the Wolfenstein parametrization. As mentioned in Subsection A of this section, the value of q^2 is conventionally chosen to be in the range $0.3 < q^2/m_b^2 < 0.5$. The CKM matrix, which should be determined from the experimental data, has the following form in term of the Wolfenstein parameters, A, λ, ρ, η [24]:

$$\begin{pmatrix} 1-\frac{1}{2}\lambda^2 & \lambda & A\lambda^3(\rho-\mathrm{i}\eta) \\ -\lambda & 1-\frac{1}{2}\lambda^2 & A\lambda^2 \\ A\lambda^3(1-\rho-\mathrm{i}\eta) & -A\lambda^2 & 1 \end{pmatrix}, \tag{27}$$

where $O(\lambda^4)$ corrections are neglected. Since λ and A are well determined and the uncertainties due to the CKM matrix elements are mostly from ρ and η, we take the central values of $\lambda(=0.225)$ and $A(=0.814)$ in the following. The range for ρ and η are:

$$\bar\rho = 0.117\pm0.021, \qquad \bar\eta = 0.353\pm0.013, \tag{28}$$

with

$$\bar\rho = \rho\left(1-\frac{\lambda^2}{2}\right), \qquad \bar\eta = \eta\left(1-\frac{\lambda^2}{2}\right).$$

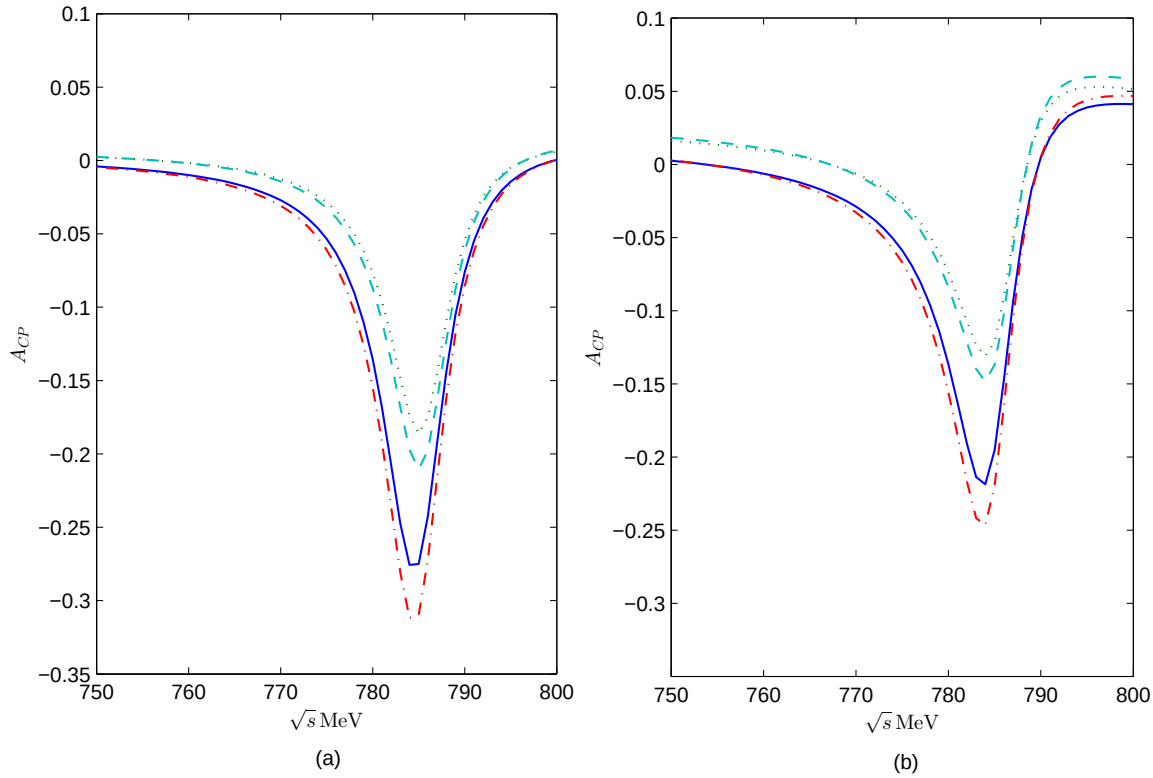

FIG. 1. The differential asymmetry, A_{CP}, in Model 1. (a) For $q^2/m_b^2 = 0.3$: Solid and dot lines correspond $N_c = 2.78$ and $N_c = 9.68$ with maximum CKM matrix elements, respectively. Dot-dashed and dashed line correspond $N_c = 2.78$ and $N_c = 9.68$ with minimum CKM matrix elements, respectively; (b) Same as (a) but for $q^2/m_b^2 = 0.5$ and $N_c = 2.85$ and 9.02.

The form factors $F_1(m_\rho^2)$ and $A_0(m_\pi^2)$ depend on the inner structure of the hadrons. Under the nearest pole dominance assumption, we take the following k^2 dependence of the form factors: for Model 1(2) [25, 26]:

$$F_1(k^2) = \frac{h_1}{1 - \frac{k^2}{m_1^2}}, \qquad A_0(k^2) = \frac{h_{A_0}}{1 - \frac{k^2}{m_{A_0}^2}}, \tag{29}$$

where $h_1 = 0.330(0.625)$, $h_{A_0} = 0.28(0.34)$, $m_1 = 5.32\,\text{GeV}$, $m_{A_0} = 5.27\,\text{GeV}$; for Model 3(4) [23, 25, 26]:

$$F_1(k^2) = \frac{h_1}{\left(1 - \frac{k^2}{m_1^2}\right)^2}, \qquad A_0(k^2) = \frac{h_{A_0}}{\left(1 - \frac{k^2}{m_{A_0}^2}\right)^2}, \tag{30}$$

where $h_1 = 0.330(0.625)$, $h_{A_0} = 0.28(0.34)$, $m_1 = 5.32\,\text{GeV}$, $m_{A_0} = 5.27\,\text{GeV}$; for Model 5 [27, 28]:

$$F_1(k^2) = \frac{h_1}{1 - x_1\frac{k^2}{m_1^2} + y_1\left(\frac{k^2}{m_1^2}\right)^2}, \qquad A_0(k^2) = \frac{h_{A_0}}{1 - x_0\frac{k^2}{m_1^2} + y_0\left(\frac{k^2}{m_1^2}\right)^2}, \tag{31}$$

where $h_1 = 0.305$, $h_{A_0} = 0.372$, $x_1 = 0.266$, $y_1 = -0.752$, $x_0 = 1.4$, $y_0 = 0.437$, $m_1 = 5.32\,\text{GeV}$, $m_{A_0} = 5.27\,\text{GeV}$. The decay constants used in our calculations are $f_\rho = f_\omega = 216\,\text{MeV}$ and $f_\pi = 132\,\text{MeV}$.

In the numerical calculations, it is found that for a fixed N_c, there is a maximum value for the differential CP violating parameter, when the low invariant mass of the $\pi^+\pi^-$ pair is near the vicinity of the ω resonance, $0.780 - 0.785\,\text{GeV}$. Five models with different form factors were investigated to study the model dependence of A_{CP} in Ref. [14]. To be more specific, in Figs. 1(a) and 1(b) we display the results for the form factors in Model 1. These results show explicitly the dependence of the CP violating asymmetry on q^2/m_b^2, CKM matrix elements and the effective parameter N_c. The dependence on N_c comes form the fact that N_c is related to the hadronization effects, and consequently, we cannot exactly determine N_c in our calculations. Therefore, we treat N_c as a free effective parameter and take it in the range $2.78(2.85) < N_c < 9.68(9.02)$ when $q^2/m_b^2 = 0.3(0.5)$ for reasons which will be explained later (Sect. III).

Then we calculate the localized integrated CP asymmetries. According to Eq. (18), we integrate A_{CP} over the low invariant mass of $\pi^+\pi^-$ ($\sqrt{s}$) and obtain the localized integrated asymmetries A_{CP}^{Ω}. Considering the significant region of ρ-ω mixing, we choose the integration interval of $\sqrt{s}$ to be from 0.750 to 0.800 GeV. In order to be consistent with the newest result of the LHCb experiments, we also calculate A_{CP}^{Ω} when $\sqrt{s}$ is in the low-mass region of the ρ^0 resonance ($0.470 < \sqrt{s} < 0.770\,\text{GeV}$) and the high-mass region ($0.770 < \sqrt{s} < 0.920\,\text{GeV}$) [6]. The numerical results are displayed in the TABLE I. We also display A_{CP}^{Ω} with and without ρ-ω mixing in TABLE II.

Table 1 shows that the values of A_{CP}^{Ω} in our calculations vary from -0.0295 (-0.0170) to -0.0860 (-0.0585) corresponding to $q^2/m_b^2 = 0.3(0.5)$, in the regions of N_c, the CKM matrix elements, and the form factors in five models when $0.750 < \sqrt{s} < 0.800\,\text{GeV}$. From Fig. 4 of Ref. [6], we can see the localized integrated CP asymmetries have different signs in $\cos\theta > 0$ and $\cos\theta < 0$ regions when $0.750 < m(\pi^+\pi^-)_{low} < 0.800\,\text{GeV}$. If one adds the events in these two experimental regions together, the total localized integrated CP asymmetry obtained from experiment becomes -0.0294 ± 0.0285 when $0.750 < m(\pi^+\pi^-)_{low} < 0.800\,\text{GeV}$. The values in our calculations agree with this experimental data. We stress that A_{CP}^{Ω} in our calculations is always negative in this integration region and its sign is model independent. We note that the signs of A_{CP}^{Ω} are positive in Models 1-4 when ρ-ω mixing is not considered

TABLE I. The localized integrated asymmetries A_{CP}^{Ω} when $q^2/m_b^2 = 0.3(0.5)$. The first line of each model corresponds to the significant region of ρ-ω mixing ($0.750 < \sqrt{s} < 0.800\,\mathrm{GeV}$). The second and third lines of each model correspond to the low-mass region ($0.470 < \sqrt{s} < 0.770\,\mathrm{GeV}$) and the high-mass region ($0.770 < \sqrt{s} < 0.920\,\mathrm{GeV}$) near the resonance mass, respectively. The second and third columns correspond to $N_c = 2.78(2.85)$. The fourth and fifth columns correspond to $N_c = 9.68(9.02)$. The second and fourth columns correspond to lower limiting values of the CKM matrix elements. The third and fifth columns correspond to upper limiting values of the CKM matrix elements.

N_c	2.78(2.85)		9.68(9.02)	
ρ, η	min	max	min	max
Model 1				
$0.750 < \sqrt{s} < 0.800\,\mathrm{GeV}$	-0.0568(-0.0438)	-0.0647(-0.0498)	-0.0320(-0.0170)	-0.0364(-0.0194)
$0.470 < \sqrt{s} < 0.770\,\mathrm{GeV}$	-0.0011(0.0086)	-0.0013(0.0098)	0.0041(0.0201)	0.0047(0.0228)
$0.770 < \sqrt{s} < 0.920\,\mathrm{GeV}$	-0.0307(-0.0082)	-0.0349(-0.0093)	-0.0157(0.0093)	-0.0179(0.0105)
Model 2				
$0.750 < \sqrt{s} < 0.800\,\mathrm{GeV}$	-0.0758(-0.0420)	-0.0859(-0.0476)	-0.0657(-0.0189)	-0.0741(-0.0214)
$0.470 < \sqrt{s} < 0.770\,\mathrm{GeV}$	0.0061(0.0424)	0.0070(0.0481)	0.0189(0.0828)	0.0212(0.0933)
$0.770 < \sqrt{s} < 0.920\,\mathrm{GeV}$	-0.0424(0.0085)	-0.0478(0.0097)	-0.0427(0.0273)	-0.0479(0.0307)
Model 3				
$0.750 < \sqrt{s} < 0.800\,\mathrm{GeV}$	-0.0569(-0.0438)	-0.0647(-0.0499)	-0.0321(-0.0170)	-0.0364(-0.0194)
$0.470 < \sqrt{s} < 0.770\,\mathrm{GeV}$	-0.0012(0.0086)	-0.0013(0.0097)	0.0041(0.0200)	0.0047(0.0228)
$0.770 < \sqrt{s} < 0.920\,\mathrm{GeV}$	-0.0305(-0.0080)	-0.0347(-0.0099)	-0.0156(0.0094)	-0.0177(0.0107)
Model 4				
$0.750 < \sqrt{s} < 0.800\,\mathrm{GeV}$	-0.0759(-0.0421)	-0.0860(-0.0477)	-0.0659(-0.0190)	-0.0742(-0.0215)
$0.470 < \sqrt{s} < 0.770\,\mathrm{GeV}$	0.0061(0.0424)	0.0069(0.0480)	0.0188(0.0828)	0.0211(0.0932)
$0.770 < \sqrt{s} < 0.920\,\mathrm{GeV}$	-0.0421(0.0089)	-0.0475(0.0100)	-0.0425(0.0277)	-0.0477(0.0311)
Model 5				
$0.750 < \sqrt{s} < 0.800\,\mathrm{GeV}$	-0.0484(-0.0514)	-0.0552(-0.0585)	-0.0295(-0.0348)	-0.0337(-0.0396)
$0.470 < \sqrt{s} < 0.770\,\mathrm{GeV}$	-0.0064(-0.0139)	-0.0074(-0.0159)	-0.0047(-0.0119)	-0.0054(-0.0136)
$0.770 < \sqrt{s} < 0.920\,\mathrm{GeV}$	-0.0273(-0.0247)	-0.0311(-0.0281)	-0.0168(-0.0172)	-0.0192(-0.0196)

in TABLE II. This indicates that ρ-ω mixing is vital for A_{CP}^{Ω} to be negative in this region.

From TABLE II, we can see ρ-ω mixing changes the sign of A_{CP}^{Ω} from positive to negative in Models 1-4 and makes A_{CP}^{Ω} be more negative in Model 5 in its significant region. Figs. 1(a) and 1(b) show that the peak of the differential asymmetry A_{CP} involving ρ-ω mixing is on the right of 0.770 GeV. Therefore, comparing with A_{CP}^{Ω} in the range $0.470 < \sqrt{s} < 0.770\,\mathrm{GeV}$, the localized integrated CP asymmetries move towards the negative direction when $0.770 < \sqrt{s} < 0.920\,\mathrm{GeV}$ due to ρ-ω mixing. This behavior is model independent. In fact, in our calculations the difference between the localized integrated CP asymmetries in the regions $0.470 < \sqrt{s} < 0.770\,\mathrm{GeV}$ and $0.770 < \sqrt{s} < 0.920\,\mathrm{GeV}$ varies from 0.0053 to 0.0688. We add the experimental events for positive and negative $\cos\theta$ in the regions $0.470 < m(\pi^+\pi^-)_{low} < 0.770\,\mathrm{GeV}$ and $0.770 < m(\pi^+\pi^-)_{low} < 0.920\,\mathrm{GeV}$ and obtain the A_{CP}^{Ω} as 0.0508 ± 0.0171 and -0.0256 ± 0.0202, respectively, from the data in TABLE IV of Ref. [6]. We can see they have opposite signs. When $0.470 < \sqrt{s} < 0.770\,\mathrm{GeV}$ and $0.770 < \sqrt{s} < 0.920\,\mathrm{GeV}$, the values of A_{CP}^{Ω} with ρ-ω mixing shown in TABLE I differ a lot among Model 1 (or 3), Model 2 (or 4), and Model 5. A_{CP}^{Ω} is also sensitive to the choice of q^2/m_b^2. When $0.470 < \sqrt{s} < 0.770\,\mathrm{GeV}$, it appears that A_{CP}^{Ω} varies from 0.0424 to 0.0933 in Models 2 and 4 for $q^2/m_b^2 = 0.5$. This result is consistent with the experimental data. When $0.770 < \sqrt{s} < 0.920\,\mathrm{GeV}$, A_{CP}^{Ω} varies from -0.0157 to -0.0349, from -0.0424 to -0.0479, from -0.0156 to -0.0347, from -0.0421 to -0.0477, and from -0.0168(-0.0172) to -0.0311(-0.0281) in Model 1 corresponding to $q^2/m_b^2 = 0.3$, in Model 2 corresponding to $q^2/m_b^2 = 0.3$, in Model 3 corresponding to $q^2/m_b^2 = 0.3$, in Model 4 corresponding to $q^2/m_b^2 = 0.3$, and in Model 5 corresponding to $q^2/m_b^2 = 0.3(0.5)$, respectively. These results are also consistent with the experimental data.

From above discussions, we can see A_{CP}^{Ω} with ρ-ω mixing, especially the signs, agree with the experimental result when $0.750 < \sqrt{s} < 0.800\,\mathrm{GeV}$. We also find that the localized integrated CP asymmetries move towards the negative direction due to ρ-ω mixing. A_{CP}^{Ω} in the region $0.770 < \sqrt{s} < 0.920\,\mathrm{GeV}$ contains the contribution of ρ-ω mixing while that in the region $0.470 < \sqrt{s} < 0.770\,\mathrm{GeV}$ dose not. Therefore, ρ-ω mixing contributes to the sign change of CP asymmetry around the $\rho^0(770)$ peak of $m(\pi^+\pi^-)_{low}$. Our results in these two regions are consistent with the experimental data for serval choices of q^2/m^2 and models of form factors. One should take the effect of ρ-ω mixing into account in order to answer the question why the sign of CP asymmetry changes around the $\rho^0(770)$ peak of $m(\pi^+\pi^-)_{low}$.

TABLE II. The localized integrated asymmetries A_{CP}^{Ω} with and without ρ-ω mixing for $q^2/m_b^2 = 0.3(0.5)$ when $0.750 < \sqrt{s} < 0.800\,\mathrm{GeV}$. The first and second lines of each model correspond to A_{CP}^{Ω} with and without ρ-ω mixing, respectively. The second and third columns correspond to $N_c = 2.78(2.85)$. The fourth and fifth columns correspond to $N_c = 9.68(9.02)$. The second and fourth columns correspond to lower limiting values of the CKM matrix elements. The third and fifth columns correspond to upper limiting values of the CKM matrix elements.

N_c	2.78(2.85)		9.68(9.02)	
ρ, η	min	max	min	max
Model 1				
with ρ-ω mixing	-0.0568(-0.0438)	-0.0647(-0.0498)	-0.0320(-0.0170)	-0.0364(-0.0194)
without ρ-ω mixing	0.0059(0.0219)	0.0068(0.0249)	0.0091(0.0308)	0.0103(0.0350)
Model 2				
with ρ-ω mixing	-0.0758(-0.0420)	-0.0859(-0.0476)	-0.0657(-0.0189)	-0.0741(-0.0214)
without ρ-ω mixing	0.0173(0.0638)	0.0195(0.0722)	0.0332(0.1121)	0.0372(0.1260)
Model 3				
with ρ-ω mixing	-0.0569(-0.0438)	-0.0647(-0.0499)	-0.0321(-0.0170)	-0.0364(-0.0194)
without ρ-ω mixing	0.0060(0.0219)	0.0068(0.0249)	0.0091(0.0309)	0.0103(0.0351)
Model 4				
with ρ-ω mixing	-0.0759(-0.0421)	-0.0860(-0.0477)	-0.0659(-0.0190)	-0.0742(-0.0215)
without ρ-ω mixing	0.0173(0.0639)	0.0195(0.0723)	0.0333(0.1122)	0.0372(0.1261)
Model 5				
with ρ-ω mixing	-0.0484(-0.0514)	-0.0552(-0.0585)	-0.0295(-0.0348)	-0.0337(-0.0396)
without ρ-ω mixing	-0.0013(-0.0048)	-0.0015(-0.0055)	-0.0017(0.0057)	-0.0019(-0.0065)

III. EXTRADITION OF N_c FROM DATA OF BRANCHING RATIOS

A. Formalism

As mentioned before, N_c includes nonfactorizable effects which are difficult to deal with at present. Therefore, we treat N_c as an effective parameter to be determined by the experimental data. With the factorized decay amplitudes, we can calculate the decay rates by using the following expression [23]:

$$\Gamma(B \to VP) = \frac{|\vec{p}_\rho|^3}{8\pi m_V^2}\Big|\frac{A(B \to VP)}{\epsilon^* \cdot p_B}\Big|^2, \tag{32}$$

where

$$|\vec{p}_\rho| = \frac{\sqrt{[m_B^2 - (m_V + m_P)^2][m_B^2 - (m_V - m_P)^2]}}{2m_B} \tag{33}$$

is the c.m. momentum of the decay particles, and $A(B \to VP)$ is the decay amplitude. In our case, to be consistent, we should also take into account the ρ-ω mixing contribution when we calculate the branching ratio since we are working to the first order of isospin violation. Explicitly, for $B^+ \to \rho^0\pi^+$, we obtain,

$$\begin{aligned} BR(B^+ \to \rho^0\pi^+) = \frac{G_F^2|\vec{p}_\rho|^3}{16\pi\Gamma_{B^+}}\Big|&[V_{ud}V_{ub}^* A_{\rho^0}^T - V_{td}V_{tb}^* A_{\rho^0}^P]/(\epsilon^* \cdot p_B) \\ &+[V_{ud}V_{ub}^* A_{\omega}^T - V_{td}V_{tb}^* A_{\omega}^P]/(\epsilon^* \cdot p_B)\frac{\tilde{\Pi}_{\rho\omega}}{(s_\rho - m_\omega^2) + \mathrm{i}m_\omega\Gamma_\omega}\Big|^2, \end{aligned} \tag{34}$$

where the tree and penguin amplitudes are

$$\begin{aligned} A_{\rho^0}^T &= a_1 X^{(B^+\rho^0,\pi^+)} + a_2 X^{(B^+\pi^+,\rho^0)}, \\ A_{\rho^0}^P &= \Big(-a_4 + \frac{3}{2}a_7 + \frac{3}{2}a_9 + \frac{1}{2}a_{10}\Big)X^{(B^+\pi^+,\rho^0)} \\ &\qquad + \Big[a_4 + a_{10} - 2(a_6 + a_8)\frac{m_\pi^2}{(m_u + m_d)(m_b + m_u)}\Big]X^{(B^+\rho^0,\pi^+)}, \\ A_{\omega}^T &= a_1 X^{(B^+\omega,\pi^+)} + a_2 X^{(B^+\pi^+,\omega)}, \\ A_{\omega}^P &= \Big[2a_3 + a_4 + 2a_5 + \frac{1}{2}(a_7 + a_9 - a_{10})\Big]X^{(B^+\pi^+,\omega)} \\ &\qquad + \Big[a_4 + a_{10} - 2(a_6 + a_8)\frac{m_\pi^2}{(m_u + m_d)(m_b + m_u)}\Big]X^{(B^+\omega,\pi^+)}. \end{aligned} \tag{35}$$

For $B^0 \to \rho^+\pi^-$, we obtain

$$BR(B^0 \to \rho^+\pi^-) = \frac{G_F^2|\vec{p}_\rho|^3}{16\pi\Gamma_{B^0}}|(V_{ub}V_{ud}^* A_{\rho^+}^T - V_{tb}V_{td}^* A_{\rho^+}^P)/(\epsilon^* \cdot p_B)|^2, \tag{36}$$

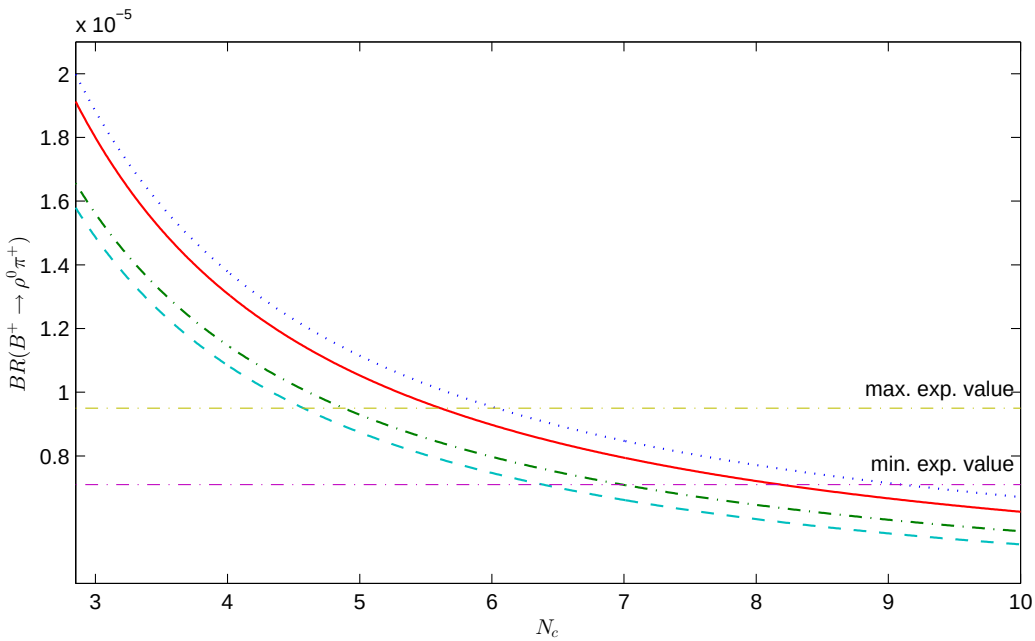

FIG. 2. The branching ratio for $B^+ \to \rho^0\pi^+$ in Model 2. Solid (dashed) line stands for $q^2/m_b^2 = 0.3$ and maximum (miximum) CKM matrix elements. Dot (dot-dashed) line stands for $k^2/m_b^2 = 0.5$ and maximum (miximum) CKM matrix elements.

where

$$\begin{aligned} A^T_{\rho^+} &= a_1 X^{(B^0\pi^+,\rho^-)}, \\ A^P_{\rho^+} &= (a_4 + a_{10}) X^{(B^0\rho^-,\pi^+)}, \end{aligned} \tag{37}$$

where $X^{(B^0\rho^+,\pi^-)} = 2 f_\pi m_\rho A_0(m_\pi^2)(\epsilon^* \cdot p_B)$ and $X^{(B^0\pi^-,\rho^+)} = \sqrt{2} f_\rho m_\rho F_1(m_\rho^2)(\epsilon^* \cdot p_B)$.

B. Numerical results

The latest experimental data of branching ratios of $B^+ \to \rho^0\pi^+$ and $B^0 \to \rho^+\pi^-$ from Particle Data Group (PDG) are [24]

$$\begin{aligned} BR(B^+ \to \rho^0\pi^+) &= (8.3 \pm 1.2) \times 10^{-6}, \\ BR(B^0 \to \rho^+\pi^-) &= (2.3 \pm 0.23) \times 10^{-5}. \end{aligned}$$

We can determine the range of N_c by comparing the theoretical values of the branching ratios with those of two body decay channels. We calculate the branching ratios with the

TABLE III. Summary of the ranges of N_c which are determined from the experimental data for various models and input parameters [numbers outside (inside) brackets are for $q^2/m_b^2 = 0.3(0.5)$]. The notation (number, number) means the lower and upper limits for N_c. (-, -) means that there is no range of N_c which is consistent with the experimental data.

	B^+	B^0
Model 1		
ρ_{max}, η_{max}	(3.70, 6.40) [(3.80, 6.71)]	(-, -) [(-, -)]
ρ_{min}, η_{min}	(2.78, 4.30) [(2.85, 4.46)]	(-, -) [(-, -)]
Model 2		
ρ_{max}, η_{max}	(5.58, 8.12) [(6.00, 9.02)]	(0.60, 0.70) [(0.62, 0.73)]
ρ_{min}, η_{min}	(4.50, 6.35) [(4.86, 6.94)]	(0.68, 0.83) [(0.72, 0.90)]
Model 3		
ρ_{max}, η_{max}	(4.08, 7.52) [(3.95, 7.12)]	(-, -) [(-, -)]
ρ_{min}, η_{min}	(3.02, 4.83) [(2.94, 4.65)]	(-, -) [(-, -)]
Model 4		
ρ_{max}, η_{max}	(6.33, 9.68) [(5.86, 8.65)]	(0.61, 0.71) [(0.66, 0.79)]
ρ_{min}, η_{min}	(5.10, 7.37)[(4.76, 6.70)]	(0.71, 0.85) [(0.66, 0.79)]
Model 5		
ρ_{max}, η_{max}	(-,-) [(-,-)]	(-,-) [(-,-)]
ρ_{min}, η_{min}	(-,-) [(-,-)]	(-,-) [(-,-)]

formula given in Eqs. (32), (34), and (36) in five models for the weak form factors which are mentioned in the previous subsection. In Fig. 2, we show the results for $B^+ \to \rho^0\pi^+$ in Model 2 as an example. The numerical results are sensitive to uncertainties coming from the experimental data. In addition, the branching ratio also depends on the CKM matrix elements which are parameterized by λ, A, ρ, and η. In the allowed ranges for the parameters ρ and η, we obtain the range of N_c. We summarize the allowed range of N_c in TABLE. III. It is found that the experimental data constrain the value of N_c into two regions. We note that if N_c approaches to zero, nonperturbative effects would be very large. Considering this, we drop the range $N_c < 1$. Therefore, N_c could be in the range $2.78(2.85) < N_c < 9.68(9.02)$ for $q^2/m_b^2 = 0.3(0.5)$. These values have been used in Section II.

IV. CONCLUSION AND DISCUSSION

The first aim of the present work is to study the localized integrated CP asymmetry for the decays $B^{\pm} \to \rho^0(\omega)\pi^+ \to \pi^+\pi^-\pi^{\pm}$ with the inclusion of ρ-ω mixing. The second aim is to study the sign change caused by ρ-ω mixing.

In the calculation of CP violating asymmetry parameters, we need the Wilson coefficients for the tree and penguin operators at the scale m_b. We worked with the renormalization scheme independent Wilson coefficients. One of the major uncertainties in our calculations is due to the fact that hadronic matrix elements of both tree and penguin operators involve nonperturbable effects. We worked in the factorization approximation, with N_c being treated as an effective parameter to include nonperturbative QCD contributions. We compared our theoretical results with the latest experimental data from PDG to determine the range of N_c as $2.78(2.85) < N_c < 9.68(9.02)$ for $q^2/m_b^2 = 0.3(0.5)$. It has been pointed out that the factorization approach is quite reliable in energetic weak decays [30].

We explicitly showed that the CP violating asymmetry is very sensitive to N_c, the CKM matrix elements and the form factors. There is a maximum value for the differential CP violating parameter when the low invariant mass of the $\pi^+\pi^-$ pair is near the vicinity of the ω resonance, $0.780 - 785\,\mathrm{GeV}$. We determined the range of the localized integrated CP asymmetry with and without ρ-ω mixing in the ranges of N_c, the CKM matrix elements, and q^2/m_b^2. For all the models investigated, we found that the localized integrated CP violating asymmetry with ρ-ω mixing varies from -0.0295 (-0.0170) to -0.0860 (-0.0585) corresponding to $q^2/m_b^2 = 0.3(0.5)$ when $0.750 < m(\pi^+\pi^-)_{low} < 0.800\,\mathrm{GeV}$. If one adds the events in the $\cos\theta < 0$ and $\cos\theta > 0$ experimental regions together when $0.750 < m(\pi^+\pi^-)_{low} < 0.800\,\mathrm{GeV}$, the total localized integrated CP asymmetry is -0.0294 ± 0.0285. Our results, especially the signs, agree with the experimental data when $0.750 < m(\pi^+\pi^-)_{low} < 0.800\,\mathrm{GeV}$. We note that the signs are positive in Models 1-4 in TABLE II when ρ-ω mixing is not considered. This indicates that ρ-ω mixing is vital for A_{CP}^{Ω} to be negative in this region. It was shown that the maximum localized integrated asymmetry in the range $0.750 < \sqrt{s} < 0.800\,\mathrm{GeV}$ can reach -0.0860. We also found that ρ-ω mixing can make the localized integrated CP asymmetries move towards the negative direction, and therefore contributes to the sign change around the $\rho^0(770)$ peak of $m(\pi^+\pi^-)_{low}$. This behavior is model independent. In our calculations, the difference between the localized integrated

CP asymmetries in the regions $0.470 < \sqrt{s} < 0.770\,\mathrm{GeV}$ and $0.770 < \sqrt{s} < 0.920\,\mathrm{GeV}$ varies from 0.0053 to 0.0688. Our results by including the ρ-ω mixing mechanism in the these two regions around the $\rho^0(770)$ peak ($0.470 < m(\pi^+\pi^-)_{low} < 0.770\,\mathrm{GeV}$ and $0.770 < m(\pi^+\pi^-)_{low} < 0.920\,\mathrm{GeV}$) are consistent with the experimental results for some models of form factors.

At this stage, we cannot explain the LHCb experimental data in the regions of positive and negative $\cos\theta$ individually. This is because three-body decays of heavy mesons are more complicated than two-body decays as they receive more contributions from different mechanisms, for example, nonresonants [31], the interference between intermediate resonances, and final-state $KK \longleftrightarrow \pi\pi$ rescattering. We will investigate the angle distribution of A_{CP}^{Ω} when considering both the ρ-ω mixing mechanism and the interference between different spin intermediate resonances [7]. We will also apply more accurate data in the future to further decrease the uncertainties in the calculations. With parameters with smaller uncertainties, we expect to be able to obtain the effects of ρ-ω mixing more precisely. This is important to interpret the angle distribution and the sign change of the CP asymmetry around the $\rho^0(770)$ peak of $m^2(\pi^+\pi^-)_{low}$ more accurately.

V. ACKNOWLEDGE

This work was supported in part by National Natural Science Foundation of China (Project Nos. 11175020, 11275025 and 11447021).

---

[1] J.H. Christenson, J.W. Cronin, V.L. Fitch, and R. Turlay, Phys. Rev. Lett. **13**, 138 (1964).

[2] N. Cabibbo, Phys. Rev. Lett. **10**, 531 (1963).

[3] M. Kobayashi and T. Maskawa, Prog. Theor. Phys. **49**, 652 (1973).

[4] Jussara M. de Miranda on behalf of the LHCb collaboration, Proceedings of CKM 2012, the 7th International Workshop on the CKM unitarity, University of Cincinnati (USA), 28 September- 2 October 2012. arXiv:1301.0283 [hep-ex].

[5] R. Aaij et al. (LHCb Collaboration), Phys. Rev. Lett. **112**, 011801 (2014).

[6] R. Aaij et al. (LHCb Collaboration), Phys. Rev. D **90**, 112004 (2014).

[7] Z.-H. Zhang, X.-H. Guo, and Y.-D. Yang, Phys. Rev. D **87**, 076007 (2013).

[8] Z.-H. Zhang, X.-H. Guo, and Y.-D. Yang, arXiv:1308.5242 [hep-ph].

[9] B. Bhattacharya, M. Gronau, and J.L. Rosner, Phys. Lett. B **726**, 337 (2013).

[10] I. Bediaga, T. Frederico, and O. Lourenco, Phys. Rev. D **89**, 094013 (2014).

[11] R. Enomoto and M. Tanabashia, Phys. Lett. B **386**, 413 (1996).

[12] S. Gardner, H.B. O'Connell, and A.W. Thomas, Phys. Rev. Lett. **80**, 1834 (1998).

[13] X.-H. Guo and A.W. Thomas, Phys. Rev. D **58**, 096013 (1998); **61**, 116009 (2000).

[14] X.-H. Guo, O. Leitner, and A.W. Thomas, Phys. Rev. D **63**, 056012 (2001).

[15] C. Wang, X.-H. Guo, Y. Liu, and R.-C. Li, Eur. Phys. J. C **74**, 3140 (2014).

[16] G. Buchalla, A.J. Buras, and M.E. Lautenbacher, Rev. Mod. Phys. **68**, 1125 (1996).

[17] N.G. Deshpande and X.-G. He, Phys. Rev. Lett. **74**, 26 (1995).

[18] R. Fleischer, Int. J. Mod. Phys. A **12**, 2459 (1997); Z. Phys. C **62**, 81 (1994); **58**, 483(1993).

[19] I. Bediaga, G. Guerrer, and J.M. de Miranda, Phys. Rev. D **76**, 073011 (2007).

[20] H.B. O'Connell, A.W. Thomas, and A.G. Williams, Nucl. Phys. A **623**, 559 (1997); K. Maltman, H.B. O'Connell, and A.G. Williams, Phys. Lett. B **376**, 19 (1996).

[21] S. Gardner and H.B. O'Connell, Phys. Rev. D **57**, 2716 (1998).

[22] M. Wirbel, B. Stech, and M. bauer, Z. Phys. C **29**, 637 (1985).

[23] Y.-H. Chen, H.-Y. Cheng, B. Tseng, and K.-C. Yang, Phys. Rev. D **60**, 094014 (1999).

[24] K.A. Olive et al. (PDG Collaboration), Chin. Phys. C **38**, 090001 (2014).

[25] M. Bauer, B. Stech, and M. Wirbel, Z. Phys. C **34**, 103 (1987).

[26] X.-H. Guo and T. Huang, Phys. Rev. D **43**, 2931 (1991).

[27] P. Ball, J. High Energy Phys. **9809**, 005 (1998).

[28] P. Ball and V.M. Braun, Phys. Rev. D **58**, 094016 (1998).

[29] G. Kramer, W.F. Palmer, and H. Simma, Nucl. Phys. B **428**, 77 (1994).

[30] H.-Y. Cheng, Phys. Lett. B **335**, 428 (1994); **395**, 345 (1997); H.-Y. Cheng and B. Tseng, Phys. Rev. D **58**, 094005 (1998).

[31] H.-Y. Cheng and C.-K. Chua, Phys. Rev. D **88**, 114014 (2013).